https://doi.org/10.5194/egusphere-2024-2644
Preprint. Discussion started: 5 September 2024

Assimilation of L-band InSAR snow depth retrievals for improved snowpack quantification

Prabhakar Shrestha[1] and Ana P. Barros[1]

[1]Department of Civil and Environmental Engineering, University of Urbana-Champaign, Urbana, Illinois, USA.

Corresponding Author: Ana P. Barros (barros@illinois.edu)

https://doi.org/10.5194/egusphere-2024-2644
Preprint. Discussion started: 5 September 2024

Abstract

The integration of snow hydrology models and remote sensing observations via data assimilation is a promising method to capture the dynamics of seasonal snowpacks at high spatial resolution and reduce uncertainty with respect to snow water resources. In this study, we employ a modified interferometric Synthetic Aperture Radar (InSAR) technique to quantify snow depth change using modeled snow density and assimilate the referenced and calibrated retrievals into a multilayer snow hydrology model (MSHM). Although the impact of assimilating snow depth change is local in space and time, the impact on snowpack mass properties (snow depth or SWE) is cumulative, and the InSAR retrievals are valuable to improve snowpack simulation and capture the spatial and temporal variability of snow depth or SWE. Details in the estimation algorithm of InSAR snow depth or SWE changes, referencing and calibration prove to be important to minimize errors during data assimilation.

https://doi.org/10.5194/egusphere-2024-2644
Preprint. Discussion started: 5 September 2024

1 Introduction

Remote sensing and distributed modelling of snowpack with data assimilation is a promising methodology to quantify snow water resources (including condition) and reduce uncertainty. Current and upcoming snow remote sensing using Synthetic Aperture Radar (SAR) aim to provide global coverage at hyper-resolution, which is needed to quantify snow variability with reduced uncertainty. Recent studies have either mostly used backscatter approaches (Lievens et al., 2019, 2022; Singh et al., 2024; Tsang et al., 2021) or interferometric SAR (InSAR) techniques(Guneriussen et al., 2001) to quantify snow depth and snow water equivalent (SWE). The latter have been applied extensively for SWE retrievals from dry snowpacks using ground-based (e.g. Leinss et al., 2015; Ruiz et al., 2022)and satellite-based SARs (e.g. Conde et al., 2019; Dagurov et al., 2020; Deeb et al., 2011; Guneriussen et al., 2001; Lei et al., 2023; H. Li et al., 2016; S. Li & Sturm, 2002; Liu et al., 2017). The InSAR technique assumes that the volume backscatter and absorption of microwave signal in the snowpack are negligible with the backscatter at the ground-snowpack interface being dominant while refraction results in phase delay. Previous studies have shown also that the InSAR retrievals are more suitable at longer wavelengths (e.g., L-band), owing to transparency of dry snow, preservation of coherence for longer periods of time and larger threshold for phase wrapping. With the upcoming NASA-ISRO (Indian Space Research Organization) SAR (NISAR) mission, multiple studies with airborne L-band UAVSAR (Uninhabited Aerial Vehicle Synthetic Aperture Radar) data have already demonstrated the potential of InSAR for snow remote sensing (e.g. Bonnell et al., 2024; Deeb et al., 2021; Hoppinen et al., 2023; Idowu and Marshall, 2022; Marshall et al., 2021; Palomaki and Sproles, 2023; Tarricone et al., 2022).

InSAR retrieval algorithms need spatial data of snow density and referencing to

https://doi.org/10.5194/egusphere-2024-2644
Preprint. Discussion started: 5 September 2024

estimate the spatial variability in absolute snow depth or snow water equivalent (SWE). Leinss et al. (2015) have proposed a modified InSAR technique to circumnavigate the need of snow density in SWE retrievals by introducing an additional parameter with very small variability for a range of incidence angles and snow density, their approach also assumes that the vertical profile of snow density does not change between the two dates for each InSAR pair. However, the density profiles can change depending on the time interval between revisits, new snowfall events, and weather conditions that may impact the top layer of the snowpack. Furthermore, snow density might still be needed in referencing the retrievals to obtain absolute snow depth or SWE for assimilation purposes. Hyper-resolution snow hydrology models driven by realistic hydrometeorological forcing can potentially provide a good estimate of snow density for the InSAR algorithm, and in turn the assimilation of InSAR retrievals can potentially improve the modeled snowpack states. Earlier studies have already shown the potential of assimilating retrieval of snow depth or SWE from airborne or satellite SAR to improve modeled snowpack and reduce uncertainty (e.g.Girotto et al., 2024; Pflug et al., 2024; Shrestha and Barros, 2024).The upcoming launch of the NASA-ISRO SAR (NISAR) mission that will provide L-band measurements globally provides impetus to investigate the assimilation of InSAR retrievals and associated uncertainty quantification with potential application to operational water prediction. Here, we leverage the multiple in-situ and airborne snow measurements available from NASA's SnowEx'20 (Marshall et al., 2019) campaign over Grand Mesa to 1) evaluate L-band InSAR retrievals of snow depth, and 2) assimilate the retrievals into a distributed snow hydrology model to evaluate the impact on the simulated macro-physical snow properties and their uncertainties. We evaluate the L-band InSAR retrievals at their native resolution over different snow depths and land covers against ground-based measurements and airborne Lidar (Light Detection and Ranging) retrievals. The InSAR

https://doi.org/10.5194/egusphere-2024-2644
Preprint. Discussion started: 5 September 2024

retrievals with the common first flight date with available observed spatial snow depth measurements were used for assimilation at different time windows and the other retrievals were used to evaluate the ensemble snow hydrology model prediction of snow properties and to characterize the impact of assimilating the InSAR retrievals of snow depth.

2 Methods

2.1 Study Area

The study area is located over the western part of Grand Mesa plateau, Colorado, USA (GM domain; Fig. 1). The land cover is dominated by grassland and mixed forests across the plateau with elevations ranging from 3000 to 3200 m. There are several scattered open water bodies (e.g., lakes and reservoirs), as well as areas with shrubs and wetlands. During the SnowEx'20 campaign, Grand Mesa was used to host an Intensive Observation Period (IOP) during the snow-on season, including bi-weekly UAVSAR flights and airborne Lidar data collections.

2.2 Data

2.2.1 UAVSAR

UAVSAR is a fully polarimetric L-band synthetic aperture radar designed to obtain high quality airborne repeat pass interferometry (Hensley et al., 2008; Rosen et al., 2006). The radar operates at a frequency of 1.26 GHz ($\lambda = 0.2379\ m$) with a bandwidth of 80 MHz, and is mounted on the NASA NASA Gulfstream III, flying at a nominal altitude of 13800 m. UAVSAR data are available from the ASF-DAAC for multiple campaigns (https://api.daac.asf.alaska.edu/services/utils/mission_list). The uavsar_pytools (https://github.com/SnowEx/uavsar_pytools) was used to download

https://doi.org/10.5194/egusphere-2024-2644
Preprint. Discussion started: 5 September 2024

and convert InSAR georeferenced binary grid files to geotiffs in WGS84 for Grand Mesa (SnowEx'20). The interferometric data consists of the interferogram, coherence, unwrapped phase in quad polarizations, including the digital elevation and incidence angles along the flight path. In some cases, all polarizations were not available. There were 7 InSAR pairs available based on 5 UAVSAR flights for repeated flight paths at a heading of 274° (Table 1). The interval between the InSAR pairs varied between 7 to 40 days (e.g. track 3-5 (11d), 3-8 (18d), 3-13 (25d),3-17 (40d),5-8 (7d),8-13 (7d) and 13-17 (15d)).

2.2.2 Snow Pit and Snow Pole Measurements

The snow pit data include measurements of snow temperature, snow depth, snow density, snow stratigraphy, snow grain size, liquid water content, and snow water equivalent over Grand Mesa. The SNEX20_GM_SP collection (Vuyovich et al., 2021) has 154 snow pit measurements between 27 January and 12 February 2020. Similarly, the SNEX20_TS_SP collection(Mason et al., 2024) has time-series of snow pit measurements between October 2019 and May 2020, obtained by the SnowEx community during the 2020 campaign.

The snow pole data (SNEX20_SD_TLI**)** consists of snow depth measurements based on time-lapse imagery by capturing a snow pole in each imagery(Breen et al., 2022). The temporal coverage for these data is from 29 September 2019 through 10 June 2020. The cameras took either three images daily (11AM, 12 PM, 1PM) or twice daily (11AM and 12PM). The cameras were placed in the Grand Mesa based on a combination of tree-density map (treeless, sparse and dense) and reference snow depths from Airborne Snow Observatory (ASO) Lidar retrievals on 8 Feb 2017 (shallow, intermediate and deep). The error estimates for each camera vary and range from ± 2 to ± 16 cm.

https://doi.org/10.5194/egusphere-2024-2644
Preprint. Discussion started: 5 September 2024

2.2.3 ASO

The Airborne Snow Observatory(ASO; Painter et al., 2016) Lidar derived snow depths at 3 m and 50 m resolution for Grand Mesa were available for Feb 1/2 (fused together) and Feb 13 during the SnowEx'20 campaign. The snow depths over forested area represent snow depths at the ground. SWE estimates were also available from ASO at 50 m resolution, based on bias corrected snow density using a snow hydrology model at 50 m resolution. The reported uncertainty in the data was 5.8 cm and 1.7 cm at 3 m resolution for the two dates, and less than 1 cm at 50 m resolution for both dates. In the ASO retrievals for SWE, the snow density was obtained by calibrating the modelled density with ground-based observations.

2.2.4 Atmospheric data

The High-Resolution Rapid Refesh (HRRR;Dowell et al., 2022) 3 km first hour forecast data for water year 2020, was downloaded using a python package (https://doi.org/10.5281/zenodo.4567540). The HRRR ensemble consists of 36 members for DA and 9 members for forecast run but were not available in the servers except the single forecast. This HRRR data were used both to estimate atmospheric correction of InSAR phase and as offline atmospheric forcing for the snow hydrology model. The HRRR grids interpolated to regular geographic grids are also outlined in the GM domain (Fig. 1).

2.3 InSAR snow depth retrieval

The total interferometric phase difference obtained with repeat pass SAR data over a snow-covered region includes contributions due to phase impacts from flat Earth, local topography, atmospheric delay, snowpack, and random and systematic errors. While the random error mostly comes from the temporal decorrelation,

https://doi.org/10.5194/egusphere-2024-2644
Preprint. Discussion started: 5 September 2024

assuming that phase impacts from flat Earth, local topography and systematic errors are accounted for in the UAVSAR InSAR processing chain, the extraction of the phase contribution only requires accurate estimation of phase contribution due to atmospheric delay (see Appendix A1). With known InSAR phase difference ($\Delta\emptyset_s$) due to the presence of snowpack, the change in snow depth (Δz_s) can be estimated following Guneriussen et al. (2001) for coherent reflections:

$$\Delta z_s = -\left(\frac{\lambda}{4\pi}\right)\frac{\Delta\emptyset_s}{\left(cos\theta_i - \sqrt{\varepsilon - sin^2\theta_i}\right)} \tag{1}$$

where λ is the SAR wavelength, θ_i is the incidence angle and ε is the bulk snowpack permittivity. For dry snow, $\varepsilon^{"}$ is negligible compared to ε' and the relationship between snow density ρ_s [kgm^{-3}] and permittivity can be expressed according to Matzler, (1996) and Wiesmann and Mätzler (1999) as follows:

$$\varepsilon = 1 + 1.6 * 10^{-3}\rho_s + 1.8 * 10^{-9}\rho_s^3 \tag{2}$$

Interferometric coherence is important to assess the uncertainty in the retrievals of snow depth, as the retrieval errors increase with decreases in coherence. Ruiz et al. (2022) used a ground based 1-10 GHz SAR system with InSAR capabilities to examine the environmental impact on the observed coherence for snow covered surface. For example, increases in air temperature leading to snow melt are associated with large drops in snow coherence, besides wind, precipitation and large changes in temperature gradients. Compared to X, C and S-band, L-band measurements exhibit higher coherence over longer temporal baselines, and lower error in SWE retrieval, indicating better suitability for InSAR applications.

The estimation of Δz_s following Eq. (1) assumes that the density of the snowpack is uniform with depth and that the underlying profile does not change with time. The latter assumption is problematic as the snow density of the underlying profile could change due to physical processes (e.g. compaction) depending on the temporal

https://doi.org/10.5194/egusphere-2024-2644
Preprint. Discussion started: 5 September 2024

baseline of the repeat pass and fresh snow. Besides, natural snowpacks are characterized by multi-layer vertical stratigraphy with varying snow density and the phase delay is an integral of the phase delay over the multiple layers (Liens et al. 2015). Using $\Delta SWE = \sum_{j=1}^{N} \Delta z_{s,j} \rho_s, j/\rho_w$, where ρ_w is the density of water, and i=1,N are the multiple layers, Liens et al. (2015) proposed a linear relationship between InSAR phase change and SWE change as follows:

$$\Delta SWE = -\Delta\emptyset_s \left(\frac{\lambda}{2\pi\alpha}\right)\left(1.59 + \theta_i^{\frac{5}{2}}\right)^{-1} \quad 3$$

where α is an optimal correction factor ranging from $0.92 - 1.07$ for a wide range of incidence angles (up to 65°) and snow densities (up to 900 kgm^{-3}). With this formulation and using an optimal α, they estimated a maximum error of 10%. To reduce the uncertainty in snow density, the above method could be directly used to estimate changes in SWE. However, errors due to variations in density profile tied to the temporal baseline between the repeat passes remain to be addressed.

Since we evaluate the model results with snow depth measurements from the lidar and ground-based measurements, we employ Eq. 1 for the estimation of snow depth change in this study. Using the atmospherically corrected unwrapped phase images from the UAVSAR data, the snow depth was retrieved over the GM domain in the native grid resolution (approx. 5 m) using average bulk snow density between two repeat pass dates from MSHM reference runs. Note that the estimated change in snow depth is also well below the limit for possible phase wrapping effect in L-band, which is around 69 cm for $\lambda = 23.6\ cm\ and\ \theta_i = 23°$ (Deeb et al., 2011). Here, it is also important to note that the estimated change in snow depth is a relative change, and without a snow-free scene or known point change in snow depth, it's not possible to relate the relative change in snow depth to absolute snow depth change. Previous

https://doi.org/10.5194/egusphere-2024-2644
Preprint. Discussion started: 5 September 2024

studies (e.g. Bonnell et al., 2024; Conde et al., 2019; Hoppinen et al., 2023; Palomaki and Sproles, 2023; Tarricone et al., 2022) have used different methods (e.g. finding pixels with no changes or using pixels with known changes) to calibrate the InSAR retrievals to obtain absolute change in snow depth or SWE. In this study we use the snow pole measurements over grasslands for the calibration. For cases, where the measurements cannot be collocated due to missing retrievals, we use the snow pole measurement over the sparsely forested areas. In addition, we use an average over a 3x3 square box in the UAVSAR scene to reduce any uncertainty due to GPS location of snow pole measurements.

2.4 MPDAF and Experiment Setup

The Multi-Physics Data Assimilation Platform (MPDAFv1.0; Shrestha and Barros, 2024) employs a coupled framework of Multilayer Snow Hydrology Model (MSHMv3.0; Cao and Barros, 2020; Kang and Barros, 2011b, 2011a; Shrestha and Barros, 2024) and the NCAR Data Assimilation Research Testbed (DART; Anderson et al., 2009; DART, 2023). MSHM is a distributed 1D-column model, that solves the mass and energy budgets of the snowpack. Key physical processes of snow hydrology - snow/rain partitioning, snow accumulation, compaction, melting, melt-runoff including snow microstructure evolution are well represented in the model to simulate the macroscopic and microscopic snow properties. More details about the parameterizations can be inferred from the studies mentioned above. Following Cao & Barros (2020), the snow albedo is provided externally using the NLDAS Mosaic Land Surface Model L4 v2.0 albedo data (Xia et al., 2012a; Xia et al., 2012b).

In DART, we use the Ensemble Adjustment Kalman Filter (EAKF;Anderson, 2003) with enhanced spatially varying state space inflation (Anderson, 2009; El Gharamti, 2018). Assimilation is carried out with observed integrated quantities like total SWE or

https://doi.org/10.5194/egusphere-2024-2644
Preprint. Discussion started: 5 September 2024

total snow depth, and the increments are then distributed vertically to the model states (snow depth, snow density and SWE) using a repartition algorithm(Shrestha & Barros, 2024). Besides, the cutoff radius that determines the region of spatial impact of the assimilated variable was set at approximately 100 m (close to the model resolution).

The snow hydrology model is setup over the GM domain using approximately 90 m resolution with 66×165 grid points. The maximum number of snow layers in the model was set to 30. The merged atmospheric forcing data are also interpolated to regular geographic grid and disaggregated to 90 m resolution. Here, no downscaling algorithms are applied to the forcing data and the disaggregation technique applies homogeneous forcing over the subgrid pixels – this also allows us to highlight the impact of hyper-resolution data assimilation.

The MSHM reference run (CTRL) was integrated from Oct 1, 2019, to Apr 1, 2020 using the default HRRR forcing data. For data assimilation (DA) runs, 48 ensemble members were generated by perturbing the model forcing data. The precipitation is perturbed using multiplicative noise drawn from a uniform distribution U[−0.4, 0.4]. The incoming shortwave and longwave are also perturbed using a multiplicative noise from a uniform distribution U[−0.05, 0.05] and U[−0.1, 0.1] respectively.

Figure 2 synthesizes the availability of ASO Lidar retrievals and L-band InSAR retrievals for assimilation and evaluation of model runs. Here, we use part of the data for assimilation and the remainder are used for evaluation. As stated earlier, the L-band InSAR retrievals only provide information about relative changes in snow depth or SWE, which need to be referenced and calibrated to obtain absolute values needed for assimilation. In the context of distributed modelling at a given resolution, this would require a spatial map of snow depth or SWE for referencing. In this study, we use the ASO Lidar snow depth data at 50 m resolution (Feb 1) as a reference and combine them with aggregated InSAR retrievals of snow depth change I1 (Feb 1-12) , I2 (Feb

https://doi.org/10.5194/egusphere-2024-2644
Preprint. Discussion started: 5 September 2024

1-19) and I3 (Feb 1-26) at 50 m resolution to obtain the absolute snow depth pattern over the GM domain on Feb 12, 19 and 26 respectively. Two DA experiments are conducted by assimilating total snow depth: 1) ASO Lidar retrieval on Feb 1, and 2) ASO Lidar retrieval on Feb 1 and referenced InSAR retrievals on Feb 12,19 and 26. We reference the InSAR retrievals by aggregating the data to 50 m resolution grid of the ASO Lidar retrievals from Feb 1, which matches the date of the first InSAR pair in both cases. InSAR retrievals of snow depth change on I5 (Feb 12-19), I6 (Feb 19-26) and I7 (Feb 26-Mar12) are reserved for independent evaluation. In both DA experiments, we assign an observational error of 10 % for the snow depth retrievals at 50 m resolution, that is consistent with the errors from the InSAR retrievals using the UAVSAR data in this study.

3 Results

3.1 Meteorological Settings

The meteorological conditions based on the HRRR forcing data including air temperature, precipitation and wind speed were analysed for the GM domain (2*5 HRRR grids at 3 km resolution). These environmental forcings along with temporal baselines are also the source of variability in interferometric coherence and errors in the retrievals. Figure 3 shows the time-series of air temperature, wind speed and precipitation intensity for the month of February including the first two weeks in March for the NW corner of the GM domain. The month of February was generally cold and windy with temperatures dropping below -20 °C, and wind speeds reaching up to 15 m/s. The time-series show cooling and warming periods at a weekly time scale, with some days where the air temperature reached above zero. However, the amplitude of cooling decreases gradually from the end of February to mid-March with more frequent

https://doi.org/10.5194/egusphere-2024-2644
Preprint. Discussion started: 5 September 2024

warm periods. There were a few snowfall events between Feb 1-12, Feb 19-26 and Feb 26-Mar 12, which varied in intensity along the GM domain.

3.2 Snow Density

A spatial pattern of bulk snow density is required to compute the snowpack permittivity needed for the InSAR retrieval technique. Uncertainty in snow density estimates can lead to errors in snow depth retrieval. Figure 4 shows the snow density distribution for the InSAR pair (Feb 1-12) using the 50 m resolution ASO Lidar data, snow pit data and model estimates using a reference run (CTRL) for the GM domain. Only the snow pit data within GM domain collected within ± 1 day of the InSAR flights were used for analysis. All three data sets show compaction of snow between the two dates, but the model simulates slightly higher snow density for both flight dates and underestimates the spatial variance as observed in the snow pit data and ASO Lidar data as expected given the coarse resolution of the HRRR precipitation forcing (i.e. 3km). Note that the snow density in ASO Lidar data is also from a model estimate but it was bias corrected (i.e., locally calibrated) using the snow pit data from SnowEX'20 campaign. In the 11-day temporal baseline, the average snow density changes by 5.6 %, 11 % and 4 % respectively among the lidar, snow pit and model data.

To examine the error in snow depth retrieval associated with error in density, we used Eq. 1 to retrieve snow depth change for a fixed phase change due to snow. Figure 4d shows the variability in InSAR retrieval of snow depth change as a function of incidence angle, for a phase change of -0.17π using the average snow density from ASO Lidar, snow pit and the MSHM CTRL run. The error generally decreases with increasing incidence angle. The synthetic simulation shows that a 10 % error in snow density can lead to approximately 10 % error in snow depth estimates at lower incidence angles, everything else being the same.

https://doi.org/10.5194/egusphere-2024-2644
Preprint. Discussion started: 5 September 2024

3.3 L-band retrieval of snow depth

The temporal baselines for the L-band retrieval range from 7 to 40 days, and the interferometric coherence generally decreased with increasing temporal base lines as expected. For treeless and forested areas, the mean coherence for 7-day temporal baseline (Feb 12-19) was 0.7 ± 0.15 and 0.65 ± 0.18 respectively. Similarly, for the Feb 19-26 pair, it was 0.6 ± 0.18 to and 0.5 ± 0.2 respectively. The coherence decreased to 0.39 ± 0.16 and 0.36 ± 0.17 for the 40-day temporal baseline. These values are for the HH polarization, as it was available for all dates. The lower coherence for the Feb 19-26 pair compared to Feb 12-19 pair could be attributed to environmental factors, e.g., larger wind speeds, precipitation event, and intermittent warming (see Fig. 3). The forested area exhibits lower coherence than the treeless area suggesting possible higher uncertainty in the retrievals. The above statistics are based on the NLCD landcover data at 30 m resolution, whereas the native resolution of InSAR retrievals from UAVSAR is in the order of 5 m resolution, and the retrievals over forest contain information from snow depth in tree clearings as well.

3.3.1 Evaluation with ASO Lidar data

The InSAR pair of Feb 1-12 with a temporal baseline of 11 days provides the closest concurrent pair with the ASO Lidar retrieval based on Feb1/2 and Feb 13 to compare the snow depth difference at a scale of 3-5 m resolution. Figures 5a-b show the spatial pattern of interferometric coherence and snow depth change at VV polarization. Figure 5c shows the change in snow depth based on ASO Lidar data for the same region. The western part of this GM subdomain is mostly dominated by snow cover over grasslands, while the eastern part contains snow cover in forested areas with relatively lower coherence. Both the Lidar and L-band retrieval capture the wavy roll like pattern due to scouring and drifting of snow over the grasslands shown earlier

https://doi.org/10.5194/egusphere-2024-2644
Preprint. Discussion started: 5 September 2024

by Marshall et al. (2021) for a smaller area. Over the eastern part of the subdomain, which is dominated by forest, there are significant discrepancies: in regions with no snow depth change in the ASO Lidar data, a decrease in snow depth is observed in the L-band retrieval.

The average coherence values for this subdomain were 0.51, 0.46, 0.39 and 0.39 for VV, HH, HV and VH polarization respectively. Also, the missing retrievals in the radar scene were 8, 11, 36 and 54 % of the area respectively for the different polarizations. The distribution of snow depth change for co-polarization better matches with the ASO Lidar data compared to cross-polarization (Fig. 5d). The average changes in snow depth for the scene were -2.42, -1.13 and -0.1 cm respectively for ASO Lidar and InSAR VV and HH polarizations. The HV and VH polarization show rightward and leftward shifted peaks respectively.

While the results were similar for other subdomains (not presented here), the L-band retrievals were found to show a general decrease in snow depth in the western most part of GM domain dominated by forest cover, while the Lidar data shows a contrasting increase in snow depth. Thus, the retrievals show higher uncertainty over the forest areas and further evaluation is needed.

3.3.2 Evaluation with snow pole and snow pit time-series data

The snow pole data provide a time-series of snow depth measurements for locations which are treeless or have sparse/dense trees and can be used for comparison with all available InSAR pairs over the GM domain. We use the linearly interpolated snow pole data in time to reference the InSAR retrievals in HH polarization and obtain absolute snow depth for comparison. Figure 6 shows the evaluation of referenced InSAR retrievals with snow pole data for treeless landcover: a-c), sparse trees : d-f), and dense trees : g-m). In most cases, the L-band InSAR retrievals capture

https://doi.org/10.5194/egusphere-2024-2644
Preprint. Discussion started: 5 September 2024

the trend in snow depth change very well for different landcover types. The root mean square errors (RMSE) were similar for different landcovers with approximate values of 4-6 cm. We also explored the errors in terms of InSAR pairs. The RMSEs of InSAR estimates were 5.0, 4.9, 4.4, 6.2, 7.3 and 4.2 cm respectively for Feb 1-12 (11d), Feb 1-19(18d), Feb 1-26(25d), Feb 12-19(7d), Feb 19-26(7d) and Feb 26-Mar 12(18d) retrievals at the 12 stations. The errors in InSAR retrievals are within 4-8 % of the absolute snow depth.

The time-series from snow pits in the north-western part of the GM domain also provide valuable snow depth measurements to evaluate the InSAR estimates. The time-series contains data across treeless and forest areas (Fig. 7). Here, again we use the snow pit measurements to reference the InSAR retrievals and obtain the absolute snow depth. It must be noted that snow pit measurements were carried out at different locations, but within a few meters. The snow depth was slightly higher for the treeless area compared to the forested area, which were within 0.25 km of each other. The InSAR retrievals can capture some of the trends very well, while showing contrasting results for others like for the case of the snow poles. The coherence was within 0.12-0.54 and 0.42-0.79 for the treeless and forested areas, respectively. The forested areas exhibited higher coherence for these measurements, and the errors were 2-9 % and 3-31% respectively for treeless and forest areas. Based on the two comparisons of InSAR retrievals against snow pole and snow pit data, the errors are within 10 % for most of the retrievals with few exceptions.

3.4 Data Assimilation and Evaluation

In this section, we explore the impact of assimilating L-band InSAR retrievals on modeled SWE and particularly modeled snow depth. As already discussed in Section 2.4, we use two assimilation experiments including an open loop (without assimilation)

https://doi.org/10.5194/egusphere-2024-2644
Preprint. Discussion started: 5 September 2024

and a reference run to explore the time evolution of modeled snowpack over Grand Mesa for the accumulation season in the water year 2020. Figure 8 shows the time-series of spatially averaged modeled snow depth from the different runs. The spatial averaging was done for the grids without trees and open water over the GM domain. The dotted lines indicate the total spread of the ensemble runs. The assimilation of the ASO lidar snow depth on Feb 1 shifts the ensembles upwards and reduces the spread for both DA and DAU runs. It shows that the reference run (CTRL) was largely underestimating snow depth. While some of the ensemble members with positive perturbation of precipitation of precipitation were able to capture the actual snow depth, the ensembles with negative perturbation of precipitation underestimated the total snow depth (see the spread in OL run). The assimilation of referenced InSAR retrievals for Feb 12, 19 and 26 (DAU runs) exhibit a small increase in snow depth for the ensemble averages compared to DA runs.

The modeled snowpack was also compared with in-situ measurements to assess the impact of data assimilation. The modeled snow depth and SWE at 90 m resolution were compared to snow pit data (IOP and TSD) in locations without trees. The land cover filtered IOP data contained snow depth and SWE from 28 Jan 2020 to 12 Feb 2020. Similarly, the land cover filtered TSD contained snow depth from 19 Dec 2019 to Apr 17, 2020. There were 68 IOP and 12 TSD snow pit data available for comparison across the GM domain based on the model simulation spatial extent. The RMSE decreased from 35.2 cm to 18.3 cm for snow depth, and for SWE it decreased from 8.9 cm to 5.9 cm. The differences in RMSE between DA and DAU runs for these pits were negligible. The modeled snow depth was also compared against snow pole measurements for locations without trees (3 locations, W1A, W1B and W3A) for the entire model simulation period. The RMSE were 17.6, 21.2 and 27.2 cm for the CTRL run, and decreased to 8.1, 21, and 20.8 cm for the DA runs. For DAU runs, the rmse

https://doi.org/10.5194/egusphere-2024-2644
Preprint. Discussion started: 5 September 2024

were 8.5, 22.2 and 19.2 cm respectively.

The spatial pattern of the modeled snow depth can be evaluated using the reserved InSAR retrievals from Feb 12-19, Feb 19-26 and Feb 26-Mar12 pairs, that were not used for assimilation. Figure 9 shows the spatial pattern of snow depth change for these repeat pass retrieval dates along with their distribution for the entire GM domain. The estimates are shown for the retrievals and all the model runs. The InSAR data were aggregated to 90 m resolution for comparison. And the grids with open water bodies and tree covers (sparse or dense) were all masked out. Additionally, for the ensemble runs, the spatial maps were obtained by averaging the ensembles, and the distributions are for the averaged ensembles.

The InSAR retrievals for Feb 12-19 and Feb 19-26 exhibit both increase and decreases in snow depth for the GM domain, while the retrievals for Feb 26-Mar 12 show increase in snow depth only (Fig. 9a-c). As expected, the ensemble average for the open loop (OL) run shows spatial variability at the scale of the atmospheric forcing. but shows similar tendency except for Feb 12-19 pair, where it shows decrease in snow depth (Fig. 9d-f). While the DA runs improve the total snow depth and SWE, no improvement in the snow depth change is achieved for the Feb 12-19 pair (Fig. 9g). In addition, there are more grids with decrease in snow depth for the remaining two pairs (Fig. 9h-i) compared to the OL run. Note that the DA does increase the modeled spatial variability in snow depth change.

Compared to other model runs, DAU produces best results with positive increase in snow depth change (Fig. 9j-k), also seen in the widening of the distribution in the positive direction (Fig. 9m-n). This is due to the assimilation of InSAR data on Feb 19 and 26. Since there was no assimilation of InSAR data on Mar 12, there is no improvement in the modeled snow depth change for Feb 26-Mar 12 even in DAU runs (Fig. 9i and Fig. 9l). The increase or relatively larger increase in snow depth change

https://doi.org/10.5194/egusphere-2024-2644
Preprint. Discussion started: 5 September 2024

for DAU runs (Fig. 9j-m) are mostly for the grids where the InSAR data were available for assimilation (Feb 19 and Feb 26). However, the impact of this assimilation appears local in time, and it does produce any significant improvement for the Feb 26-Mar 12 pair compared to DA runs. Despite the data constraints, these results indicate that the assimilation of InSAR estimates has the potential to improve the spatial pattern of modeled snow depth change. Because the snow depth evolution is accumulative, these changes will impact the overall seasonal evolution of the snowpack.

4 Discussion

The hyper-resolution InSAR retrievals resolve the wavy roll like patterns due to scouring and drifting of snow over the grasslands as captured by the ASO lidar data over the grasslands in the NW part of GM domain, also shown earlier by Marshall et al. (2021). However, over forested regions, there are disagreements between the lidar and the InSAR estimates with possible uncertainty in both data sets. The average coherence was similar for VV and HH polarization with slightly higher values for VV polarization and lower for HV and VH polarizations. This resulted in higher percentage of missing retrievals in cross-polarizations. The scene-wide average coherence in HH polarization for the 7-day temporal baseline (treeless area) in the GM domain is around 0.6-0.7 which is consistent with values reported by Ruiz et al. (2022). Similarly, the coherence was around 0.5-0.65 for the forested area indicating that the L-band can maintain good coherence over canopy and, with sufficient penetration depending on tree density and canopy architecture, it can be useful in measuring ground snow depth changes. The forested areas generally exhibited lower coherence as expected and the coherence differences between treeless and forested areas were around 14-23% to 8 % for 7-day and 40-day temporal baselines, respectively. Overall, the InSAR retrievals generally compare well with in-situ measurements from snow pole and snow pit over sparse and dense forests.

The interferometric coherence across the GM domain generally decreased with increasing temporal baseline (e.g. by 44 % from 7 to 40-day temporal baseline). This indicates that the retrieval uncertainty and retrieval error will increase with larger time between the repeat passes as expected. Since the underlying density of snowpack will also change between the repeat passes, the retrieval error will also increase when using a constant density in Eq. 1. In this study, the depth weighted density averages or the average bulk density between two repeat pass dates from the reference MSHM model runs were used for the InSAR retrievals. The reference runs generally underestimated the total snow depth and SWE compared to the ASO lidar data and snow pit measurements, but the bulk snow density was slightly higher than the snow pit observations during the IOP over Grand Mesa. This indicates that the HRRR forcing used for the study underestimates the snowfall events, besides model uncertainty associated with wind redistribution of snow which is not accounted for. The modelled higher bulk density could again indicate uncertainty in the fresh snow density(Cao and Barros, 2020; Shrestha and Barros, 2024) and compaction parameterization (e.g. Abolafia-Rosenzweig et al., 2024). The modelled layered snowpack generally shows a two-layer density profile, with an upper layer exhibiting a gradient and near constant density profile in the lower layer. Upon examining density profiles, the difference in snow density profile in the lower layer varied between 1.5-1.8 % (Feb 19-26) and 6-7 % (Feb 1-26) for 7-day and 25-day temporal baseline. This could be still a lower estimate than the actual change in snow density, as shown earlier for 11-day temporal baseline, which was 4 and 11 % for model and snow pit observations. Therefore, the variability in snow density profiles is small for the 7-day base line, and it is large for 25-day base line during the accumulation period. Besides the modelled density has its

https://doi.org/10.5194/egusphere-2024-2644
Preprint. Discussion started: 5 September 2024

own bias compared to actual snowpack density due to forcing and model structural uncertainty. However, the calibration of the retrievals to obtain absolute snow depth change from the relative snow depth change could also compensate for these errors. Further in-depth studies are needed to better understand the sources of error.

Data assimilation of the ASO Lidar snow depth reduces the error and uncertainty in the modeled snow depth. This also reduced the bulk snow density for the ensemble members with lower snow depth (compared to CTRL run) by 4-5 %, as new snow with lower density is added on the top by the repartition algorithm (Shrestha and Barros, 2024). These ensemble members (DA; Fig. 9h-i) also exhibited lower or negative snow depth change for Feb 19-26 and Feb 26-Mar 12 compared to OL ensembles, which is reflected in the ensemble averages over the GM domain. However, the assimilation of referenced InSAR retrievals (DAU) produces increase in snow depth changes in the ensemble average compared to DA runs. The impact is most apparent in the grids of the GM domain where the data were available for assimilation. This produced the best distribution of snow depth change compared to observations, showing the potential of InSAR retrievals in improving the modeled snowpack. It also demonstrates HRRR underestimation of snowfall between the dates of the InSAR pairs (e.g. between Feb 26 and Mar 12) and it explains the small snow depth differences in the OL runs compared to InSAR retrievals. The OL shows the increase in snow depth due to snowfall just before Mar 12 (see Fig. 3) albeit underestimated as indicated by the difference in magnitude between the InSAR retrievals and the OL snow depth changes. Likewise, the impact of assimilating InSAR retrievals which improves the simulated snow depth changes (as seen for the first two pairs) highlights the need for high temporal resolution of SAR measurements.

https://doi.org/10.5194/egusphere-2024-2644
Preprint. Discussion started: 5 September 2024

5 Conclusion

This study shows that InSAR retrievals are useful to improve the snowpack simulation and capture its spatial and temporal variability. The assimilation of hyper-resolution retrievals of snow depth is equivalent to a downscaling of precipitation forcing with a bias correction. The RMSE of the InSAR retrievals of absolute snow depth change at native resolution compared to snow pole measurements over different land covers were within 4-6 cm, which corresponds to less than 10 % of the absolute snow depth. However, reference snow depth or SWE is essential to obtain absolute snow depth or SWE for assimilation purposes, which poses a challenge in an operational context. In this situation, one would start from snow-free conditions and build up the absolute snow depth from InSAR retrievals using the prior estimates as reference. Accurate calibration of the estimated relative snow depth change, or SWE will be important to minimize retrieval errors. Future studies are needed to advance a general framework for calibrating InSAR retrievals and obtaining absolute snow depth or SWE for assimilation into the models.

https://doi.org/10.5194/egusphere-2024-2644
Preprint. Discussion started: 5 September 2024

Code availability

The MPDAF v1.0 software with experiment setups is available from https://github.com/mpdaf23/mpdaf.git. MSHM v3.0 used here is documented in Kang and Barros (2011a, 2011b); Cao and Barros (2020) including the updates described in this paper. MEMLS can be downloaded from http://www.iapmw.unibe.ch/research/projects/snowtools/memls.html. The NCAR DART can be downloaded from https://github.com/NCAR/DART.git.

Data availability

The NASA SnowEx 2020 observation data can be downloaded from NASA National Snow and Ice Data Center Distributed Active Archive Center and ASF DAAC. HRRR atmospheric forcing data can be now downloaded from Amazon Web Services (AWS) courtesy of National Oceanic and Atmospheric Administration (NOAA) and the Registry of Open Data on AWS. The NLDAS albedo data can be downloaded from the NASA GES DISC. Model data and software used for visualization is available from https://uofi.box.com/v/InSARmodeldata.

Author contribution

PS and APB conceptualized the study. PS designed the study, processed the data, conducted the model simulation with data assimilation, carried out the analysis, and wrote the paper. APB acquired the grant for the study and contributed to editing of the manuscript.

Competing interests

The authors declare that they have no conflict of interest.

https://doi.org/10.5194/egusphere-2024-2644
Preprint. Discussion started: 5 September 2024

Acknowledgements

The funding for this study was provided by the National Oceanic and Atmospheric Administration (NOAA), awarded to the Cooperative Institute for Research on Hydrology (CIROH) through the NOAA Cooperative Agreement with The University of Alabama, NA22NWS4320003. This study made use of the Illinois Campus Cluster, a computing resource that is operated by the Illinois Campus Cluster Program (ICCP) in conjunction with the National Center for Supercomputing Applications (NCSA) and which is supported by funds from the University of Illinois at Urbana-Champaign. The analysis of data was done using the NCAR Command Language (Version 6.6.2). The data used in this effort were acquired as part of the activities of NASA's Science Mission Directorate and are archived and distributed by the Goddard Earth Sciences (GES) Data and Information Services Center (DISC).

https://doi.org/10.5194/egusphere-2024-2644
Preprint. Discussion started: 5 September 2024

References

Abolafia-Rosenzweig, R., He, C., Chen, F., and Barlage, M.: Evaluating and enhancing snow compaction process in the Noah-MP land surface model, J Adv Model Earth Syst, 16, e2023MS003869, 2024.

Anderson, J.: Spatially and temporally varying adaptive covariance inflation for ensemble filters, Tellus A: Dynamic meteorology and oceanography, 61, 72–83, 2009.

Anderson, J., Hoar, T., Raeder, K., Liu, H., Collins, N., Torn, R., and Avellano, A.: The data assimilation research testbed: A community facility, Bull Am Meteorol Soc, 90, 1283–1296, 2009.

Anderson, J. L.: A local least squares framework for ensemble filtering, Mon Weather Rev, 131, 634–642, 2003.

Bonnell, R., McGrath, D., Tarricone, J., Marshall, H.-P., Bump, E., Duncan, C., Kampf, S., Lou, Y., Olsen-Mikitowicz, A., and Sears, M.: Evaluating L-band InSAR Snow Water Equivalent Retrievals with Repeat Ground-Penetrating Radar and Terrestrial Lidar Surveys in Northern Colorado, EGUsphere, 2024, 1–33, 2024.

Breen, C. M., Hiemstra, C., Vuyovich, C. M., and Mason, M.: SnowEx20 Grand Mesa Snow Depth from Snow Pole Time-Lapse Imagery, Version 1, Boulder, Colorado USA, 2022.

Cao, Y. and Barros, A. P.: Weather-dependent nonlinear microwave behavior of seasonal high-elevation snowpacks, Remote Sens (Basel), 12, 3422, 2020.

Conde, V., Nico, G., Mateus, P., Catalão, J., Kontu, A., and Gritsevich, M.: On the estimation of temporal changes of snow water equivalent by spaceborne SAR interferometry: a new application for the Sentinel-1 mission, Journal of Hydrology and Hydromechanics, 67, 93–100, 2019.

Dagurov, P. N., Chimitdorzhiev, T. N., Dmitriev, A. V, and Dobrynin, S. I.:

https://doi.org/10.5194/egusphere-2024-2644
Preprint. Discussion started: 5 September 2024

Estimation of snow water equivalent from L-band radar interferometry: simulation and experiment, Int J Remote Sens, 41, 9328–9359, 2020.

DART: The data assimilation research testbed (version 10.7.3), Boulder, Coloardo, 2023.

Deeb, E., Forster, R., Vuyovich, C., Elder, K., Hiemstra, C., and Lund, J.: L-band InSAR depth retrieval during the NASA SnowEx 2020 campaign: Grand mesa, Colorado, in: 2021 IEEE International Geoscience and Remote Sensing Symposium IGARSS, 625–627, 2021.

Deeb, E. J., Forster, R. R., and Kane, D. L.: Monitoring snowpack evolution using interferometric synthetic aperture radar on the North Slope of Alaska, USA, Int J Remote Sens, 32, 3985–4003, 2011.

Dowell, D. C., Alexander, C. R., James, E. P., Weygandt, S. S., Benjamin, S. G., Manikin, G. S., Blake, B. T., Brown, J. M., Olson, J. B., and Hu, M.: The High-Resolution Rapid Refresh (HRRR): An hourly updating convection-allowing forecast model. Part I: Motivation and system description, Weather Forecast, 37, 1371–1395, 2022.

El Gharamti, M.: Enhanced adaptive inflation algorithm for ensemble filters, Mon Weather Rev, 146, 623–640, 2018.

Girotto, M., Formetta, G., Azimi, S., Bachand, C., Cowherd, M., De Lannoy, G., Lievens, H., Modanesi, S., Raleigh, M. S., and Rigon, R.: Identifying snowfall elevation patterns by assimilating satellite-based snow depth retrievals, Science of The Total Environment, 906, 167312, 2024.

Guneriussen, T., Hogda, K. A., Johnsen, H., and Lauknes, I.: InSAR for estimation of changes in snow water equivalent of dry snow, IEEE Transactions on Geoscience and Remote Sensing, 39, 2101–2108, 2001.

Hanssen, R. F.: Radar interferometry: data interpretation and error analysis, Springer Science & Business Media, 2001.

Hensley, S., Wheeler, K., Sadowy, G., Jones, C., Shaffer, S., Zebker, H., Miller, T., Heavey, B., Chuang, E., and Chao, R.: The UAVSAR instrument: Description and first results, in: 2008 IEEE Radar Conference, 1–6, 2008.

Hoppinen, Z. M., Oveisgharan, S., Marshall, H.-P., Mower, R., Elder, K., and Vuyovich, C.: Snow Water Equivalent Retrieval Over Idaho, Part B: Using L-band UAVSAR Repeat-Pass Interferometry, The Cryosphere Discussions, 2023, 1–24, 2023.

Idowu, A. N. and Marshall, H.-P.: Snow depth retrieval from L-band data based on repeat pass InSAR techniques, in: IGARSS 2022-2022 IEEE International Geoscience and Remote Sensing Symposium, 4248–4251, 2022.

Kang, D. H. and Barros, A. P.: Observing system simulation of snow microwave emissions over data sparse regions—Part I: Single layer physics, IEEE transactions on geoscience and remote sensing, 50, 1785–1805, 2011a.

Kang, D. H. and Barros, A. P.: Observing system simulation of snow microwave emissions over data sparse regions—Part II: Multilayer physics, IEEE transactions on geoscience and remote sensing, 50, 1806–1820, 2011b.

Lei, Y., Shi, J., Liang, C., Werner, C., and Siqueira, P.: Snow Water Equivalent Retrieval Using Spaceborne Repeat-Pass L-Band SAR Interferometry Over Sparse Vegetation Covered Regions, in: IGARSS 2023-2023 IEEE International Geoscience and Remote Sensing Symposium, 852–855, 2023.

Leinss, S., Wiesmann, A., Lemmetyinen, J., and Hajnsek, I.: Snow water equivalent of dry snow measured by differential interferometry, IEEE J Sel Top Appl Earth Obs Remote Sens, 8, 3773–3790, 2015.

Li, H., Xiao, P., Feng, X., He, G., and Wang, Z.: Monitoring snow depth and its change using repeat-pass interferometric SAR in Manas River Basin, in: 2016 IEEE International Geoscience and Remote Sensing Symposium (IGARSS), 4936–4939,

https://doi.org/10.5194/egusphere-2024-2644
Preprint. Discussion started: 5 September 2024

2016.

Li, S. and Sturm, M.: Patterns of wind-drifted snow on the Alaskan arctic slope, detected with ERS-1 interferometric SAR, Journal of Glaciology, 48, 495–504, 2002.

Lievens, H., Demuzere, M., Marshall, H.-P., Reichle, R. H., Brucker, L., Brangers, I., de Rosnay, P., Dumont, M., Girotto, M., and Immerzeel, W. W.: Snow depth variability in the Northern Hemisphere mountains observed from space, Nat Commun, 10, 4629, 2019.

Lievens, H., Brangers, I., Marshall, H.-P., Jonas, T., Olefs, M., and De Lannoy, G.: Sentinel-1 snow depth retrieval at sub-kilometer resolution over the European Alps, Cryosphere, 16, 159–177, 2022.

Liu, Y., Li, L., Yang, J., Chen, X., and Hao, J.: Estimating snow depth using multi-source data fusion based on the D-InSAR method and 3DVAR fusion algorithm, Remote Sens (Basel), 9, 1195, 2017.

Marshall, H. , V. C. , H. C. , B. L. , E. K. , D. J. , and N. J.: NASA SnowEx 2020 Experiment Plan, 2019.

Marshall, H.-P., Deeb, E., Forster, R., Vuyovich, C., Elder, K., Hiemstra, C., and Lund, J.: L-band InSAR depth retrieval during the NASA SnowEx 2020 campaign: Grand mesa, Colorado, in: 2021 IEEE International Geoscience and Remote Sensing Symposium IGARSS, 625–627, 2021.

Mason, M., Marshall, H., McCormick, M., Craaybeek, D., Elder, K., and Vuyovich, C. M.: SnowEx20 Time Series Snow Pit Measurements, Version 2, Boulder, Colorado USA, 2024.

Matzler, C.: Microwave permittivity of dry snow, IEEE Transactions on Geoscience and Remote Sensing, 34, 573–581, 1996.

Painter, T. H., Berisford, D. F., Boardman, J. W., Bormann, K. J., Deems, J. S., Gehrke, F., Hedrick, A., Joyce, M., Laidlaw, R., and Marks, D.: The Airborne Snow

https://doi.org/10.5194/egusphere-2024-2644
Preprint. Discussion started: 5 September 2024

Observatory: Fusion of scanning lidar, imaging spectrometer, and physically-based modeling for mapping snow water equivalent and snow albedo, Remote Sens Environ, 184, 139–152, 2016.

Palomaki, R. T. and Sproles, E. A.: Assessment of L-band InSAR snow estimation techniques over a shallow, heterogeneous prairie snowpack, Remote Sens Environ, 296, 113744, 2023.

Pflug, J. M., Wrzesien, M. L., Kumar, S. V, Cho, E., Arsenault, K. R., Houser, P. R., and Vuyovich, C. M.: Extending the utility of space-borne snow water equivalent observations over vegetated areas with data assimilation, Hydrol Earth Syst Sci, 28, 631–648, 2024.

Rosen, P. A., Hensley, S., Wheeler, K., Sadowy, G., Miller, T., Shaffer, S., Muellerschoen, R., Jones, C., Zebker, H., and Madsen, S.: UAVSAR: A new NASA airborne SAR system for science and technology research, in: 2006 IEEE conference on radar, 8-pp, 2006.

Ruiz, J. J., Lemmetyinen, J., Kontu, A., Tarvainen, R., Vehmas, R., Pulliainen, J., and Praks, J.: Investigation of environmental effects on coherence loss in SAR interferometry for snow water equivalent retrieval, IEEE Transactions on Geoscience and Remote Sensing, 60, 1–15, 2022.

Shrestha P. and A . P. Barros: Multi-physics Data Assimilation Framework for Remotely Sensed Snowpacks to Improve Water Prediction, Water Resource Research, 2024.

Singh, S., Durand, M., Kim, E., and Barros, A. P.: Bayesian physical–statistical retrieval of snow water equivalent and snow depth from X-and Ku-band synthetic aperture radar–demonstration using airborne SnowSAr in SnowEx'17, Cryosphere, 18, 747–773, 2024.

Smith, E. K. and Weintraub, S.: The constants in the equation for atmospheric refractive index at radio frequencies, Proceedings of the IRE, 41, 1035–1037, 1953.

Tarricone, J., Webb, R. W., Marshall, H.-P., Nolin, A. W., and Meyer, F. J.: Estimating snow accumulation and ablation with L-band InSAR, The Cryosphere Discussions, 2022, 1–33, 2022.

Tsang, L., Durand, M., Derksen, C., Barros, A. P., Kang, D.-H., Lievens, H., Marshall, H.-P., Zhu, J., Johnson, J., and King, J.: Global monitoring of snow water equivalent using high frequency radar remote sensing, The Cryosphere Discussions, 2021, 1–57, 2021.

Vuyovich, C., H.P. Marshall, K. Elder, C. Hiemstra, L. Brucker, and M. McCormick: SnowEx20 Grand Mesa Intensive Observation Period Snow Pit Measurements, Version 1, NASA National Snow and Ice Data Center Distributed Active Archive Center, 2021.

Wang, X., Zeng, Q., and Jiao, J.: Utilization of WRF 3D Meteorological Data to Calculate Slant Total Delay for InSAR Atmospheric Correction, Remote Sens Earth Syst Sci, 4, 30–43, 2021.

Wiesmann, A. and Mätzler, C.: Microwave emission model of layered snowpacks, Remote Sens Environ, 70, 307–316, 1999.

Xia, Y., Mitchell, K., Ek, M., Cosgrove, B., Sheffield, J., Luo, L., Alonge, C., Wei, H., Meng, J., and Livneh, B.: Continental-scale water and energy flux analysis and validation for North American Land Data Assimilation System project phase 2 (NLDAS-2): 2. Validation of model-simulated streamflow, Journal of Geophysical Research: Atmospheres, 117, 2012a.

Xia, Y., Mitchell, K., Ek, M., Sheffield, J., Cosgrove, B., Wood, E., Luo, L., Alonge, C., Wei, H., and Meng, J.: Continental-scale water and energy flux analysis and validation for the North American Land Data Assimilation System project phase 2 (NLDAS-2): 1. Intercomparison and application of model products, Journal of

https://doi.org/10.5194/egusphere-2024-2644
Preprint. Discussion started: 5 September 2024

Geophysical Research: Atmospheres, 117, 2012b.

https://doi.org/10.5194/egusphere-2024-2644
Preprint. Discussion started: 5 September 2024

Appendix A1

The atmospheric delay experienced by a microwave signal can be estimated by integrating the atmospheric refractivity along the line of sight from the surface to the airborne sensor height. Neglecting the impact of ionosphere for the UAVSAR flying at a height of z_s, the scaled up atmospheric refractivity of moist air [N=(n-1)10^6], where n is the refractive index, is given by

$$N(x,z) = k_1 \frac{P}{T} + (k_2 - k_1)\frac{e}{T} + \; k_3 \frac{e}{T^2} + k_4 W_{cl}$$

where P is pressure [hPa], T is air temperature [K], e is vapor pressure [hPa], W_{cl} is liquid water content [kgm^{-3}], n_e is ionization and f is frequency. The remaining term are constants: $k_1 = 0.776\, KPa^{-1}$, $k_2 = 0.716\, KPa^{-1}$, $k_3 = 3750\, K^2 Pa^{-1}$, $k_4 = 1430\, m^3 kg^{-1}$. Based on the works of Smith and Weintraub (1953), the above relation is restricted to certain limits of the variables for an accuracy of 0.5 percent in N(x,z). The limits in this case restrict its use to temperatures of -50 to + 40° C, total pressures of 200 to 1100 mb, water-vapor partial pressures of 0 to 30 mb, and a frequency range of 0 to 30 GHz.

$N(x,z)$ can be further decomposed into the mean and turbulent part for a radar scene as:

$$N(x,z) = \bar{N}(z) \; + N'(x,z)$$

where $\bar{N}(z)$ is the average vertical stratification for the given resolution of the atmospheric model (here 3 km) and $N'(x,z)$ is the deviation from the average profile along the location x in the radar scene (within the atmospheric grid). Neglecting the turbulent terms, zenith delay L for the mean part can be computed as

$$L = \int_{z_{ref}}^{z_s} \left(k_1 \frac{P}{T} + (k_2 - k_1)\frac{e}{T} + \; k_3 \frac{e}{T^2}\right) dz$$

Using $dP = -\rho g dz$ and $\rho = P/R_d T$, where ρ is air density [kgm^{-3}] , $R_d =$

https://doi.org/10.5194/egusphere-2024-2644
Preprint. Discussion started: 5 September 2024

$287.053\, Jkg^{-1}K^{-1}$ is the dry gas constant, ang g is acceleration due to gravity, we obtain:

$$L = -10^{-6}\left(k_1 \frac{R_d}{g}\left(P(z_s) - P(z_{ref})\right)\right) + 10^{-6}\int_{z_{ref}}^{z_s}\left((k_2 - k_1)\frac{e}{T} + k_3\frac{e}{T^2}\right)dz$$

The first term of the right side is the hydrostatic correction term, and the second term is the wet correction term. The atmospheric phase delay along the line of sight (LOS) can then be estimated using the microwave wavelength (λ) and incidence angle (θ_{inc}) as:

$$\emptyset_{atm} = \frac{4\pi}{\lambda}\frac{L}{\cos(\theta_{inc})}$$

The above simple approximation for computing atmospheric phase delay along the LOS could introduce additional uncertainty(Wang et al., 2021). More importantly, since SAR interferograms are not sensitive to image-wide phase biases, there will be no horizontal delay differences over flat terrain. However, for a radar scene with terrain, the differences in the vertical refractivity during both acquisitions will affect phase difference between two arbitrary resolution cells with different topographic height(Hanssen, 2001). Therefore, the contribution of tropospheric stratification in the interferogram will only be present if the radar scene has resolution cells with different elevations. So, we compute the differential atmospheric phase delay between location with maximum elevation ($z_{ref} = p$) and all other locations ($z_{ref} = q$) in the radar scene for two SAR acquisition time t_1 and t_2 as:

$$\Delta\emptyset_{atm} = \frac{4\pi}{\lambda cos\theta_{inc}}\left[(L_p^{t_1} - L_q^{t_1}) - (L_p^{t_2} - L_q^{t_2})\right]$$

Then the phase change contribution due to snowpack is estimated as:

$$\Delta\emptyset_s = \Delta\emptyset_{InSAR} - \Delta\emptyset_{atm}$$

https://doi.org/10.5194/egusphere-2024-2644
Preprint. Discussion started: 5 September 2024

798 ## Tables
799
800 **Table 1:** UAVSAR flight retrieval dates for Grand Mesa during SnowEx'20 campaign.

Flight track	Acquisition Date
3	Feb 01 2020 (02:13:36 – 02:15:58 UTC)
5	Feb 12 2020 (16:47:20 – 16:49:45 UTC)
8	Feb 19 2020 (17:24:18 – 17:27:07 UTC)
13	Feb 26 2020 (17:40:54 – 17:43:34 UTC)
17	Mar 12 2020 (18:17:08 – 18:20:28 UTC)

801
802

https://doi.org/10.5194/egusphere-2024-2644
Preprint. Discussion started: 5 September 2024

Figures

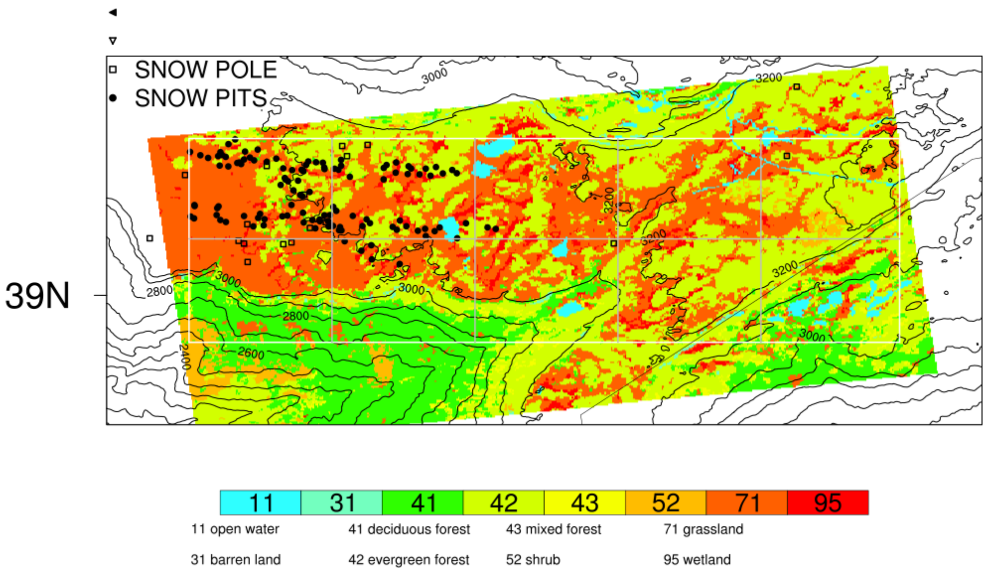

Figure 1: Spatial pattern of land cover and topography over the Grand Mesa (GM) domain (white outline). The gray boxes outline the 3 km atmospheric grids. The solid black and square markers show the location of snow pit and snow pole measurements available from SnowEx'20 campaign.

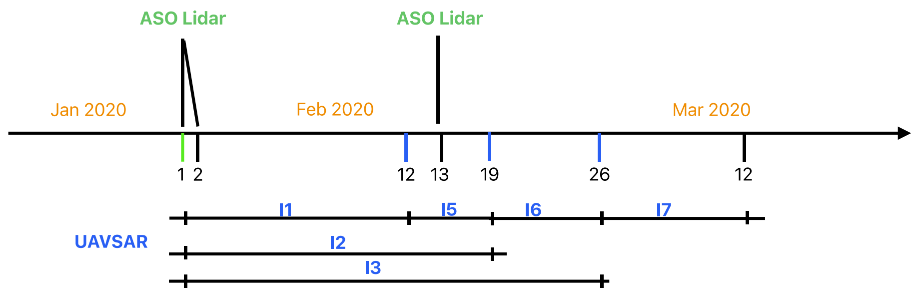

Figure 2: Timeline of availability of UAVSAR interferometric products and ASO Lidar retrievals of snow depth and SWE for SnowEx'20 campaign over Grand Mesa. I1, I2, I3 and I5, I6, I7 indicate the six InSAR pairs used for data assimilation and model evaluation respectively. The dates with green and blue tick mark represent days when the retrievals were used for assimilation in the data assimilation experiments.

https://doi.org/10.5194/egusphere-2024-2644
Preprint. Discussion started: 5 September 2024

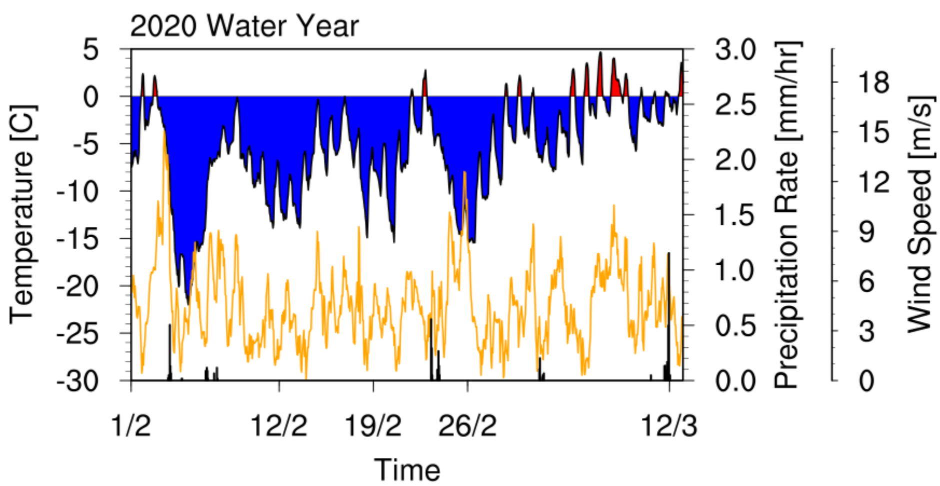

Figure 3: Meteorological data from atmospheric model for north-west GM subdomain showing air temperature (blue/red), wind speed (orange) and precipitation rate (bar plot). The time axis highlights the dates when the L-band UAVSAR flight data were available for SnowEx'20 campaign.

https://doi.org/10.5194/egusphere-2024-2644
Preprint. Discussion started: 5 September 2024

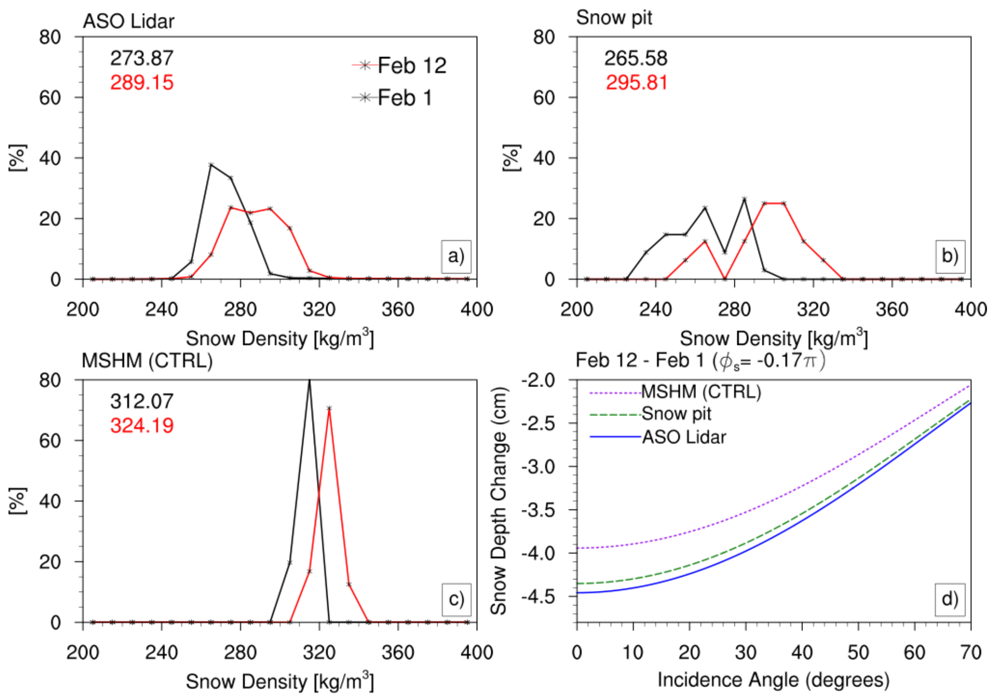

Figure 4: a-c) Snow density distribution at two different dates from the ASO Lidar data, snow pit measurements (Intensive Observation Period) and MSHM control run. **d)** Impact of snow density on the L-band InSAR retrieval of snow depth change between the two dates as a function of incidence angle for a fixed change in phase due to snowpack ($\emptyset_s = 0.17\pi$). The dates for ASO Lidar in actual are Feb 1/2 and Feb 13. We use Feb 1 and Feb 12, due to availability of InSAR phase data for these dates.

https://doi.org/10.5194/egusphere-2024-2644
Preprint. Discussion started: 5 September 2024

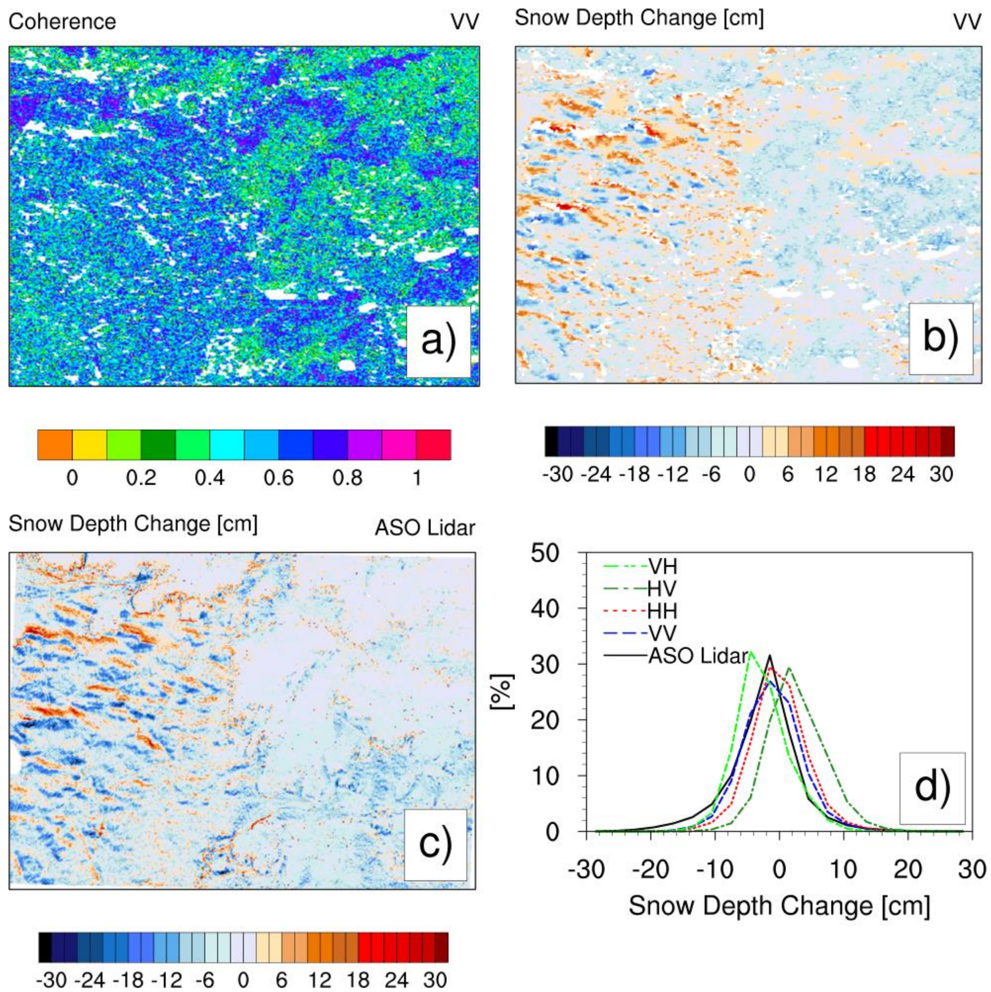

Figure 5: a) Spatial pattern of coherence from L-band VV polarization InSAR retrieval for north-west GM subdomain. **b)** Estimated spatial pattern of snow depth changes from the same retrieval. **c)** Spatial pattern of snow depth change from ASO Lidar data (Feb 1/2–13). **d)** Distribution of change in snow depth for ASO Lidar and InSAR retrievals for VV, HH, HV and VH polarizations. The InSAR retrievals were obtained from UAVSAR flight pairs for Feb 1 and Feb 12.

https://doi.org/10.5194/egusphere-2024-2644
Preprint. Discussion started: 5 September 2024

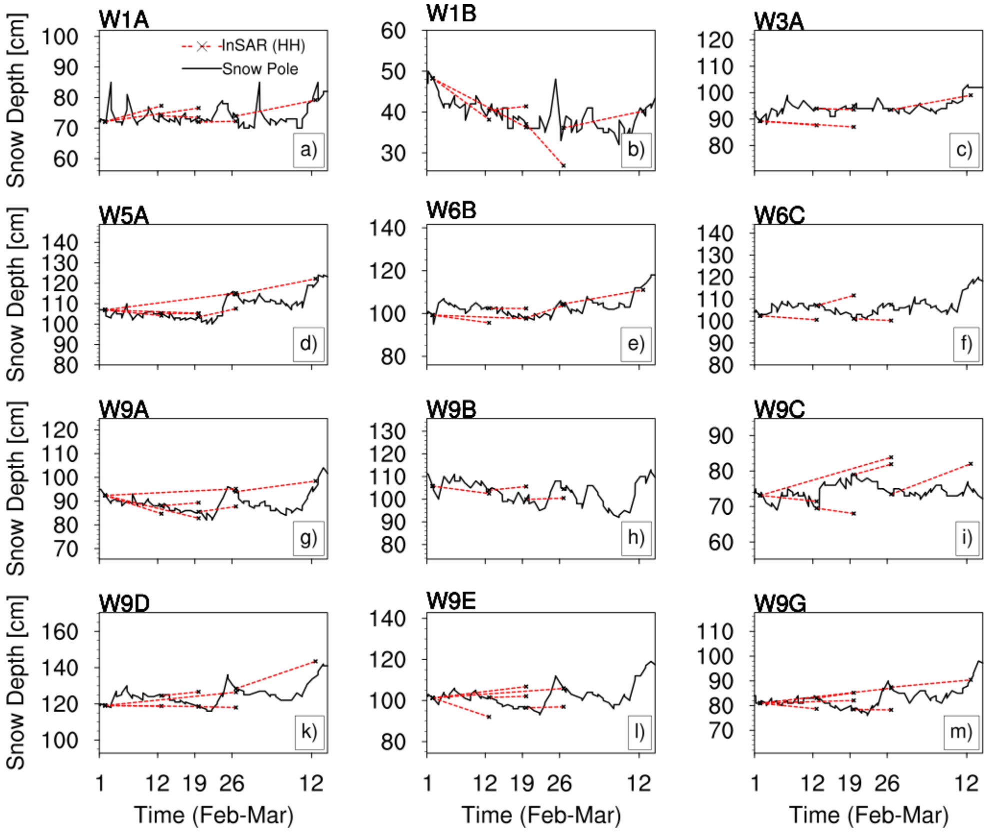

Figure 6: Comparison of L-band InSAR retrieval (HH polarization) of snow depth with Snow Pole measurements for locations with different landcover within the GM domain (**a-c:** Treeless; **d-f:** Sparse trees; **g-m:** Dense trees). For the InSAR retrieval, snow depth measurements from Snow Pole sites were used a reference for the repeat pass UAVSAR flight pairs.

https://doi.org/10.5194/egusphere-2024-2644
Preprint. Discussion started: 5 September 2024

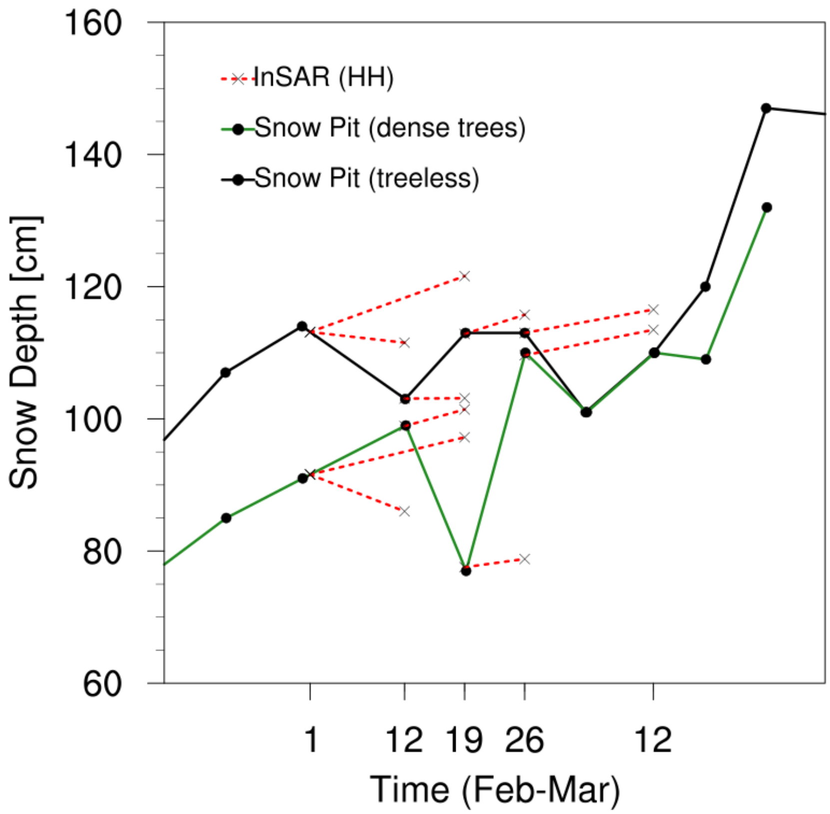

Figure 7: Comparison of L-band InSAR retrieval (HH polarization) of snow depth with snow pit time-series measurements for two locations with different landcover (treeless and dense trees) within the GM domain. For the InSAR retrieval, snow depth measurements from snow pit site were used a reference for the repeat pass UAVSAR flight pairs

https://doi.org/10.5194/egusphere-2024-2644
Preprint. Discussion started: 5 September 2024

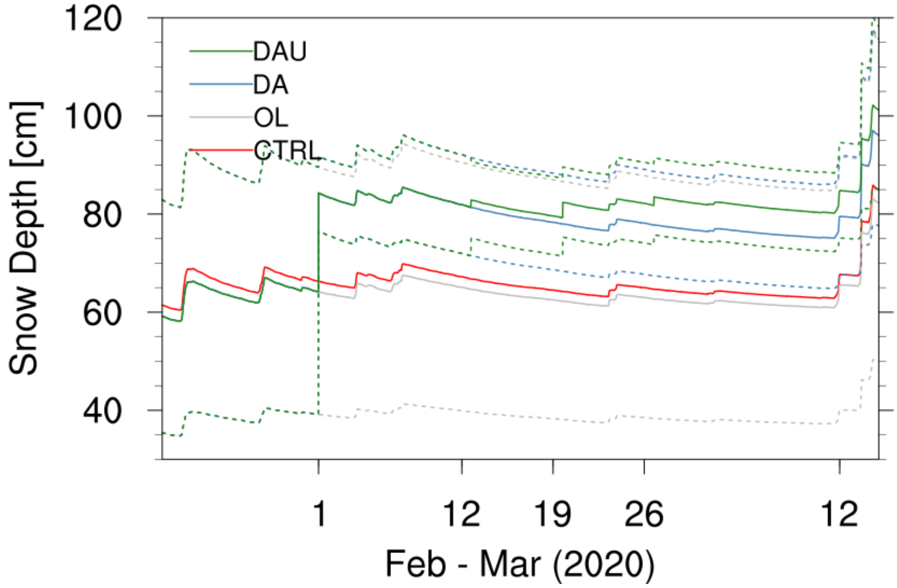

Figure 8: Time series of modeled snow depth for CTRL, OL, DA and DAU run. The dates when observation were assimilated are also shown by tick marks: DA (Feb 1) and DAU (Feb1, Feb 12 and Feb 26) are also shown by the tick marks. The ensemble spread for OL, DA and DAU runs are shown by the dotted lines.

https://doi.org/10.5194/egusphere-2024-2644
Preprint. Discussion started: 5 September 2024

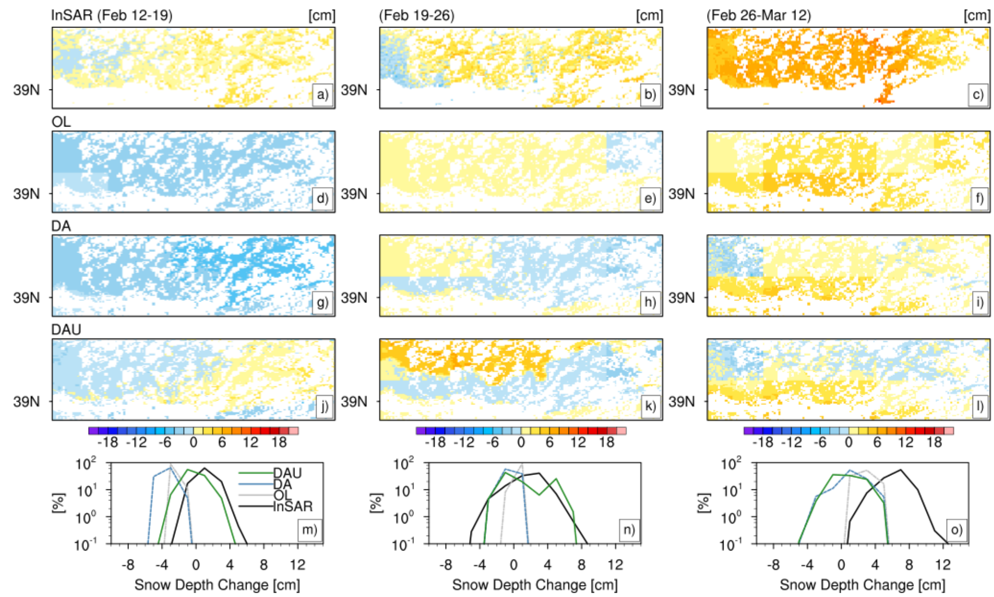

Figure 9: Spatial pattern and histogram of change in snow depth over the GM domain for Feb 12-19, Feb 19-26 and Feb 26-Mar 12: **a-c)** InSAR retrievals, **d-f)** ensemble averaged open loop run (OL), **g-i)** ensemble averaged data assimilation run with ASO Lidar data (DA), **j-l)** ensemble average data assimilation runs with ASO Lidar and referenced InSAR data (DAU), and **m-p)** frequency distribution of snow depth change for InSAR, OL, DA and DAU runs for respective pairs.